# Millennial variability and long-term changes of the diatom production in the eastern equatorial Pacific during the last glacial cycle

Oscar E. Romero,[1] Guillaume Leduc,[2] Laurence Vidal,[3] and Gerhard Fischer[4]

Received 10 December 2010; revised 24 January 2011; accepted 28 February 2011; published 13 May 2011.

[1] The modern eastern equatorial Pacific (EEP) is a major natural source for atmospheric carbon dioxide and is thought to be connected to high-latitude ocean dynamics by oceanic teleconnections on glacial-interglacial timescales. A wealth of sedimentary records aiming at reconstructing last Quaternary changes in primary productivity and nutrient utilization have been devoted to understanding those linkages between the EEP and other distant oceanic areas. Most of these records are, however, clustered in the pelagic EEP cold tongue, with comparatively little attention devoted to coastal areas. Here we present downcore measurements of the composition and concentration of the diatom assemblage together with opal (biogenic silica) concentration at site MD02-2529 recovered in the coastal Panama Basin. Piston core MD02-2529, collected in an area affected by a multitude of processes, provides evidence for strong variations in diatom production at the millennial timescale during the last glacial cycle. The maxima in total diatom concentration occurred during the early marine isotopic stage (MIS) 4 as well as during the MIS 4/3 transition and MIS 3. Rapid changes in diatom concentrations during the MIS 3 mimics Bond cycles as independently recorded by the sea surface salinity estimation derived from planktonic foraminifera from the same core. Such patterns indicate a clear linkage between diatom production in the coastal EEP and rapid climate changes in the high-latitude North Atlantic. In parallel, the long-term succession of the diatom community from coastal diatoms, predominantly thriving during MIS 5 and 4, toward pelagic diatoms, dominant during MIS 3 and 2, points to a long-term change in the surface hydrology. During Heinrich events, diatoms strongly reduced their production, probably because of enhanced stratification in the upper water column. After the last glacial maximum, diatom production and valve preservation strongly decreased in response to the advection of nutrient-depleted ($H_2SiO_4$), warmer water masses. Our high-resolution record highlights how regional climatic processes can modulate rapid changes in siliceous primary production as triggered by wind-induced local upwelling, indicating that millennial climatic variability can overtake other prominent hydrological processes such as those related to silicic acid leakage.

**Citation:** Romero, O. E., G. Leduc, L. Vidal, and G. Fischer (2011), Millennial variability and long-term changes of the diatom production in the eastern equatorial Pacific during the last glacial cycle, *Paleoceanography*, *26*, PA2212, doi:10.1029/2010PA002099.

## 1. Introduction

[2] The modern eastern equatorial Pacific (EEP) is a major natural source for atmospheric carbon dioxide and is thought to be connected to high-latitude ocean dynamics by oceanic teleconnections on glacial-interglacial timescales [*Takahashi et al.*, 1997; *Pichevin et al.*, 2009]. Past changes in the balance between carbon-rich upwelling waters and subsequent ocean productivity in that region are hence suspected to have impacted atmospheric carbon dioxide concentrations [*Pichevin et al.*, 2009]. A wealth of sedimentary records aiming at reconstructing last Quaternary changes in primary productivity and nutrient utilization in this oceanic area have been devoted to understanding the

[1]Instituto Andaluz de Ciencias de la Tierra (CSIC-UGR), Campus Fuentenueva, Facultad de Ciencias, Universidad de Granada, Granada, Spain.
[2]Universität Kiel, Kiel, Germany.
[3]CEREGE, UMR6635, CNRS Université Paul Cézanne Aix-Marseille III, Aix-en-Provence, France.
[4]Faculty of Geosciences and MARUM, University of Bremen, Bremen, Germany.


0883-8305/11/2010PA002099

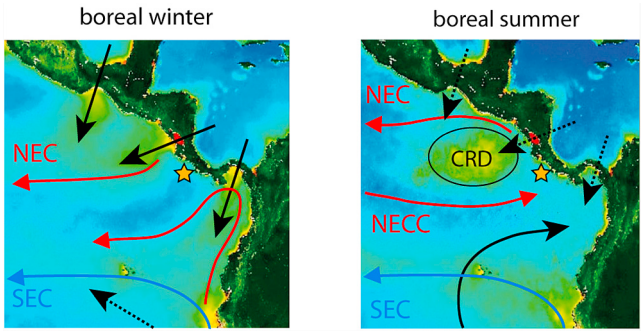


**Figure 1.** Location of site MD02-2529 (orange star) off the Costa Rican Margin in the Panama Basin. Warm (red) and cold (blue) surface currents in (left) boreal winter and (right) boreal summer are shown on SeaWIFS maps for sea surface productivity in the Eastern Equatorial Pacific Ocean (NEC, North Equatorial Current; SEC, South Equatorial Current; NECC, North Equatorial Countercurrent; CRD, Costa Rica Dome). Black arrows represent predominant wind directions blowing above low-level mountains of Central America that produce local upwelling as seen in chlorophyll filaments for the boreal winter [*Chelton et al.*, 2000]. Dotted arrows represent secondary winds. The SeaWIFS satellite pictures were obtained from http://oceancolor.gsfc.nasa.gov/cgi/biosphere_globes.pl.

linkages between the EEP and other distant oceanic areas [*Kienast et al.*, 2006; *Bradtmiller et al.*, 2006, 2009, 2010; *Pichevin et al.*, 2009; *Dubois et al.*, 2010].

[3] Paleoceanographic reconstructions for the late Quaternary in the EEP have demonstrated that glacial-interglacial climate changes were clearly imprinted in biogeochemical cycles at a regional scale as recorded in sedimentary sequences from the EEP cold tongue or in the Panama Basin [e.g., *Lea et al.*, 2003; *Robinson et al.*, 2005]. Reconstructions of past changes in primary productivity in the EEP marginal environments are also diagnostic for understanding how the interactions between the hydrological signature of climate changes and the carbon and nutrient cycles are set up [e.g., *Leduc et al.*, 2007]. However, comparatively little attention has been paid to productivity variations in marginal environments from the EEP. Such studies may, however, provide insightful information on how global surface hydrological processes linked to regional changes in climate can shape marine records for paleoproductivity from coastal environments where different processes interact.

[4] Opal sedimentary content is considered to be among the most powerful paleoproductivity proxies and has been used worldwide to estimate siliceous paleoproduction [*Cortese et al.*, 2004]. Based on the observation of low opal accumulation during the Last Glacial Maximum (LGM) beneath the EEP, which was initially considered as an area where primary productivity increased during glacial periods, *Kienast et al.* [2006] recently raised questions on past changes in silicic acid ($H_2SiO_4$) supply to low latitudes and on the reliability of downcore diatom records. Since the valves of diatom species can vary considerably in size, surface area, and silicification [*Ragueneau et al.*, 2000; *Leynaert et al.*, 2001], studying the species composition of the sedimentary diatom community in parallel with opal accumulation is pivotal in determining which processes are related to the records of diatom valves that accumulate at the seafloor [*Romero and Armand*, 2010]. The study of diatom assemblages together with morphological assessment of valve preservation has recently been proposed as an unfulfilled task to characterize the relationship between diatom production in surface waters and the burial of opal along the EEP [*Dubois et al.*, 2010]. Although several records spanning the late Quaternary opal accumulation in the pelagic EEP [*Kienast et al.*, 2006; *Bradtmiller et al.*, 2006, 2010; *Warnock et al.*, 2007; *Pichevin et al.*, 2009; *Dubois et al.*, 2010] as well as some diatom-based reconstructions for the LGM and the deglaciation along the western coast of Central and North America [*Sancetta*, 1992; *Barron et al.*, 2003, 2005; *Barron and Bukry*, 2007] are available, high-resolution reconstructions of the variability of the diatom production during the last glacial cycle from marginal environments are still lacking.

[5] To further assess hydrographic and productivity changes in the easternmost equatorial Pacific, we extend on *Leduc et al.* [2007] and reconstruct the variations in diatom production between late Marine Isotope Stage (MIS) 5 and the last deglaciation (98–10 ka B.P.) from piston core MD02-2529 retrieved in the Panama Basin (Figure 1). Our study focuses on the comparison of the concentration of diatom valves with the species composition of the diatom community, together with the monitoring of valve preservation. This is the first record of variations in diatom paleoproduction in the marginal EEP at the millennial timescale spanning the last glacial period.

## 2. Modern Eastern Equatorial Pacific Settings

[6] The westward flowing North Equatorial Current (NEC) and eastward flowing North Equatorial Counter-Current (NECC) are in geostrophic balance along the poleward and equatorward slopes, respectively, of the NECC thermocline ridge [*Fiedler and Talley*, 2006] (Figure 1). The westward flowing South Equatorial Current (SEC) flows along the equatorial thermocline ridge year-round (Figure 1). Part of the NECC is deflected north where it reaches the Central America coast and joins the Costa Rica Coastal Current (CRCC), which partly flows back into the NEC (Figure 1). This pattern of cyclonic flow exists only in summer-fall and surrounds the Costa Rica Dome (CRD) where intense primary productivity takes place [*Fiedler*, 2002] (Figure 1).

[7] Tropical Surface Water ($T > 25°$, $S < 34$) dominates north of the equator while Equatorial Surface Water ($T < 25°$, $S > 34$) dominates along the equator [*Wyrtki*, 1966]. At the core location, sea surface temperatures (SST) are higher than 27°C and sea surface salinity (SSS) is lower than 33.2 throughout the year [*Fiedler and Talley*, 2006]. Minima in local SST and their corresponding maxima in primary productivity extend offshore from the Gulfs of Tehuantepec, Papagayo, and Panama during the boreal winter (Figure 1), and are associated with seasonal wind jets blowing through Central American low-level mountain channels induced by winter high-pressure systems over the Gulf of Mexico and Caribbean Sea [*Chelton et al.*, 2000]. Those regional features are linked to surface winds and currents off western Central America that change seasonally as the ITCZ moves

north and south. The ITCZ reaches its annual southernmost extreme in February [*Fiedler*, 2002]. As the coastal shoaling of the thermocline persists offshore of the Gulfs of Tehuantepec, Papagayo, and Panama until March or April, the ITCZ migrates northward in May and the zonal band of cyclonic curl on the northern side of the ITCZ moves northward, allowing the NECC to flow eastward [*Fiedler*, 2002]. In summer, the southeast trade winds blow across the equator and are deflected eastward as far north as 8°N, providing intense rainfall over the Columbian margin [*Póveda et al.*, 2006].

[8] The CRD is associated with the terminus of the equatorial current system [*Fiedler*, 2002; *Kessler*, 2006] and is influenced by mesoscale coastal eddies [*Willett et al.*, 2006]. It appears to be formed in winter by the wind stress curl (Papagayo wind jet and westerly remnants of the SE trades) and is maintained during summer by the NECC cyclonic circulation as it reaches the Central American coast to become the CRCC. These circulation patterns result in an offshore doming of the thermocline and enhanced nutrient supply to the euphotic zone [*Fiedler*, 2002]. At the CRD location, the thermocline shoals near the sea surface, and its associated maximum of primary productivity centered at around 9°N, 90°W (i.e., nearby the MD02-2529 site) spreads regionally as the cyclonic circulation is sustained over summer months [*Fiedler*, 2002; *Fiedler and Talley*, 2006].

## 3. Material and Methods

### 3.1. Piston Core MD02-2529

[9] Core MD02-2529 (08°12.33′N; 84°07.32′W; 1619 m water depth; Figure 1) was collected during the IMAGES VIII/MD 126 MONA oceanographic cruise, off the Costa Rican margin in the Panama Basin. Since a strong decrease in diatom production together with poor valve preservation are observed after ~10 ka B.P. in the EEP, our diatom and opal study focuses on the time period 98–10 ka B.P. (352–1573 cm of MD02-2529 corrected depth).

### 3.2. Stratigraphy

[10] A detailed description of the stratigraphy of MD02-2529 is presented in *Leduc et al.* [2007] and *Leduc et al.* [2010]. The age model for core MD02-2529 is based on calibrated radiocarbon ages for the last 40 ka B.P. The 60–99 ka B.P. interval is dated by correlating the benthic $\delta^{18}O$ record to a reference stack of benthic foraminifera $\delta^{18}O$ records [*Lisiecki and Raymo*, 2005]. The mean sedimentation rate is ~13 cm $kyr^{-1}$ for MIS 2–4.

### 3.3. Diatom Countings

[11] For diatom and opal studies, around 380 samples of 1.5 $cm^3$ were taken at 2 to 4 cm intervals. The average temporal resolution averages 230 years per sample (range is 20–1193 years). Samples for diatoms were prepared following the method proposed by *Schrader and Gersonde* [1978]. Qualitative and quantitative analyses were done at ×1000 magnifications using an Olympus® BP41 microscope with phase-contrast illumination. Counts were carried out on permanent slides of acid cleaned material (Mountex® mounting medium). Several traverses across each slide were examined, depending on valve abundances, which varied between 450 and 900 valves. At least two coverslips per sample were scanned in this way. Diatom counting of replicate slides indicates that the analytical error of the concentration estimates is ≤15%. The counting procedure and definition of counting units for diatoms followed those proposed by *Schrader and Gersonde* [1978].

[12] The description of the state of preservation of the valves (Figure 2b) provides additional information for assessing how representative the preserved diatom community is and the significance of the statistical analysis (see section 3.5), as selective valve preservation may bias the results. Following observations with light microscopy, three stages of preservation were defined: (1) good: no significant enlargement of the areolae or dissolution of the valve margin can be detected; (2) moderate: delicately silicified species show areolae enlargement, dissolution of the valve margin and valve fragmentation; and (3) poor: strong dissolution of the valve margin and areolae enlargement.

### 3.4. Opal (Biogenic Silica) Measurements

[13] Samples for the analysis of opal were freeze-dried and ground in an agate mortar. Opal content was determined by the sequential leaching technique of *DeMaster* [1981], with further modifications by *Müller and Schneider* [1993].

### 3.5. Principal Components Analysis

[14] To investigate the covariability between the different diatom populations as observed in a preliminary analysis of the temporal distribution of species, a principal component analysis (PCA) was carried out by means of SPSS, Version 15.0.1 (http://www.spss.com/). The extraction of Principal Components amounts to a variance maximizing (*varimax*) rotation of the original variable space. The criterion for the rotation is to maximize the variance (variability) of the "new" variable (factor), while minimizing the variance around the new variable. Out of 153 diatom species identified in ~380 samples in core MD02-2529, the PCA covered the 27 most abundant diatom species. The average relative contribution of each of these 27 diatoms exceeds 1% for the entire period studied in this work. The diatom data set of MD02-2529 results in five factors (groups of diatoms), which account for around 83% of the original variance (Table 1).

## 4. Results

### 4.1. Variations of Total Diatom and Opal Concentrations

[15] Throughout the 98–10 ka B.P. time period, diatom concentration in the Panama Basin off the Costa Rican margin exhibits rapid variations on the millennial timescale (Figure 2a). The concentration of diatoms ranges between $5.3 \times 10^3$ and $6.1 \times 10^6$ valves $g^{-1}$ (average for the entire study period = $2.1 \times 10^6$ valves $g^{-1}$). Diatoms show maxima (above $2.5 \times 10^6$ valves $g^{-1}$) between 79 and 73, 57–53, 52–50, 45–46, and 38.5–36 ka B.P. Lowest diatom concentrations ($<1.0 \times 10^6$ valves $g^{-1}$) are recorded between 97 and 95.5, 85.5–83.5, 72–70.5, 47.5–46 ka B.P., and after 18.5 ka B.P. throughout 10 ka B.P.

[16] Preservation of diatom valves also varies strongly on the millennial timescale (Figure 2b). Overall, the valve

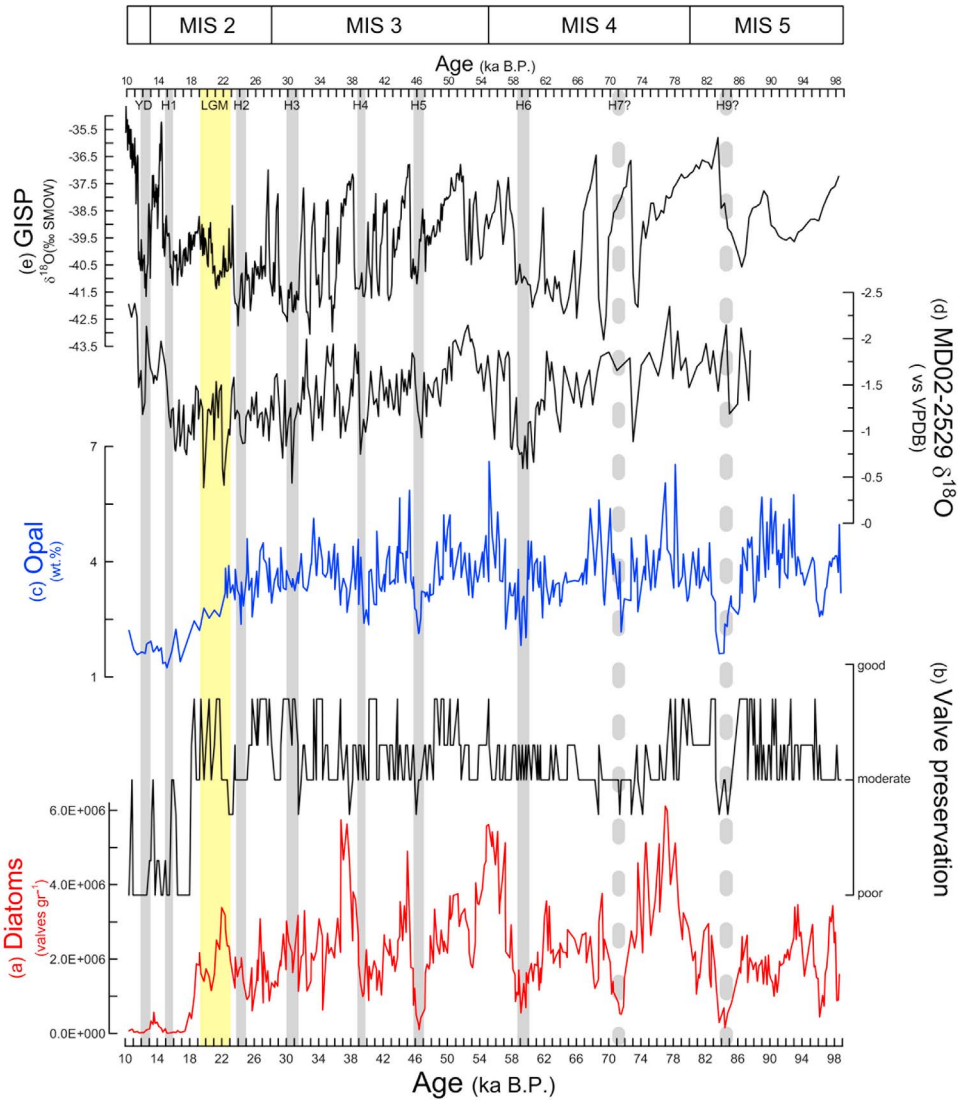


**Figure 2.** Downcore variations of (a) total diatom concentration (red line, valves $g^{-1}$), (b) the valve preservation (black line), (c) opal (blue line, wt. %), and (d) $\delta^{18}O$ (‰ VPDB) of the planktonic foraminifer *Globigerina bulloides* (black line) for the time period 98–10 ka B.P. at site MD02-2529 and (e) $\delta^{18}O$ (‰ SMOW) from Greenland (GRIP). The Last Glacial Maximum (LGM, 23.0–19.0 ka B.P.) is indicated by the yellow shading, and Heinrich events and the Younger Dryas are indicated by the gray shadings.

preservation is moderate to good between 98 and 18.5 ka B.P., while it varies from poor to moderate after 18.5 ka B.P. (Figure 2b), suggesting that the diatom signal preserved during most of the studied interval is unlikely to be driven at first-order by diatom dissolution. During periods of maximum diatom concentration, valves are mostly well preserved. Preservation of valves, however, becomes mostly moderate during periods of lowest diatom concentration (97 and 95.5, 85.5–83.5, 72–70.5, 47.5–46 ka B.P.) The strong decrease in diatom concentration after 18.5 ka B.P. is accompanied by the poorest preservation of valves for the entire studied period (Figure 2b).

[17] Opal values range between 1.5 and 6.1 wt.% at site MD02-2529 (Figure 2c). Opal shows similar temporal variations as already described for diatom valves. Maximum opal values (>4 wt.%) are seen around 93–89, 77–78, 70–67, 56–55, 45–44, 52–50, 45–46, and 35–34 ka B.P. Opal minima (<2.5 wt.%) are recorded between 97 and 95.5, 85.5–83.5, 72, 59–60, 47–46, 40 and beyond 20 ka B.P., and are mostly in phase with the occurrence of Heinrich events (HEs) (Figure 2c). Although the variations in opal content appear to be of lower amplitude than the variations in diatom valves, their timing is identical.

### 4.2. Variations in the Composition of the Diatom Assemblage

[18] At site MD02-2529, 153 diatom species were identified. Due to the high diversity of the diatom assemblages and in order to summarize the ecological information delivered by the main diatom contributors at site MD02-2529, we applied PCA on the relative abundance (%) of 27 diatom species. For the PCA, the relative concentration of diatoms between 98 and 18 ka B.P. was considered, since the diatom values between 18 and 10 ka B.P. are beyond the

**Table 1.** Varimax Loadings Matrix[a]

| Species | 1 | 2 | 3 | 4 | 5 |
|---|---|---|---|---|---|
| *Actinocyclus curvatulus* | −0.166 | −0.083 | **0.054** | 0.001 | −0.050 |
| *Actinoptychus senarius* | −0.060 | **0.133** | 0.086 | 0.113 | −0.052 |
| *Actinoptychus vulgaris* | **0.202** | −0.045 | 0.129 | 0.159 | 0.083 |
| *Alveus marinus* | 0.134 | 0.114 | −0.057 | 0.073 | **0.159** |
| *Azpeitia barronii* | −0.711 | −0.568 | −0.402 | 0.037 | **0.059** |
| *Azpeitia nodulifera* | −0.452 | −0.232 | −0.021 | −0.011 | **0.032** |
| *Azpeitia tabularis* | 0.112 | **0.237** | 0.156 | −0.038 | −0.001 |
| Resting spore (RS) of *Chaetoceros affinis* | 0.217 | 0.055 | **0.346** | 0.284 | −0.041 |
| RS *Chaetoceros compresus* | **0.249** | −0.021 | 0.208 | 0.231 | −0.012 |
| RS *Chaetoceros* sp. 1 | **0.384** | 0.057 | 0.243 | 0.245 | −0.080 |
| *Coscinodiscus decrescens* | −0.148 | −0.262 | −0.066 | 0.040 | **0.075** |
| *Coscinodiscus radiatus* | 0.007 | −0.124 | −0.109 | **0.024** | −0.076 |
| *Cyclotella litoralis* | −0.305 | **0.868** | −0.379 | 0.022 | 0.086 |
| *Fragilariopsis doliolus* | 0.078 | −0.112 | 0.418 | 0.044 | **0.888** |
| *Nitzschia interruptestriata* | **0.319** | −0.025 | 0.179 | −0.017 | −0.027 |
| *Paralia sulcata* | −0.356 | **0.024** | −0.019 | −0.253 | 0.012 |
| *Rhizosolenia bergonii* | 0.058 | **0.175** | 0.054 | 0.040 | 0.058 |
| *Thalassionema frauenfeldii* | 0.158 | −0.039 | **0.251** | 0.169 | 0.091 |
| *Thalassionema nitzschioides* var. *nitzschioides* | **0.879** | −0.174 | −0.437 | −0.030 | 0.058 |
| *Thalassionema nitzschioides* var. *inflata* | −0.172 | 0.079 | −0.068 | 0.077 | **0.099** |
| *Thalassionema nitzschioides* var. *parva* | 0.076 | −0.148 | **0.369** | −0.202 | 0.215 |
| *Thalassionema pseudonitzschioides* | 0.222 | 0.015 | 0.047 | **0.252** | −0.078 |
| *Thalassiosira ferelineata* | −0.055 | 0.029 | **0.258** | 0.190 | −0.039 |
| *Thalassiosira lineata* | **0.229** | −0.035 | 0.203 | −0.020 | −0.058 |
| *Thalassiosira nanolineata* | 0.190 | 0.063 | 0.121 | **0.194** | 0.059 |
| *Thalassiosira oestrupii* var. *oestrupii* | −0.104 | 0.015 | **0.017** | −0.987 | 0.008 |
| *Thalassiosira oestrupii* var. *venrickae* | −0.091 | 0.027 | **0.073** | −0.207 | 0.050 |
| Variance | 33.69 | 23.87 | 12.97 | 8.64 | 4.14 |
| Cumulative variance | 33.69 | 57.57 | 70.54 | 79.18 | 83.32 |

[a]Rotation is varimax normalized. Factor scores for analysis on ~380 samples using 27 diatom taxa with average abundance ≥1.0% of total diatom assemblage at site MD02-2529 between 98 and 18 ka B.P. Bold values indicate dominant species or group of species within each factor (loadings > 0.700). For the representation of the relative contribution of each factor (group), see Figure 3.

required statistical significance. The first five factors (groups of diatoms) explain ~83% of the total variance (Figure 3 and Table 1).

[19] The highly diverse diatom assemblage is mainly composed of species typically from open-ocean, warm to temperate waters with a secondary contribution from coastal components. As described for the total diatom concentration, the relative contribution of all diatom groups shows variations at the millennial timescale (Figure 3). Longer-term distribution patterns revealed by groups 1 and 5 cannot be linked to a clear glacial/interglacial cyclicity.

[20] Group 1 (~34% of the total variance) is predominantly composed of coastal species such as *Thalassionema nitzschioides* var. *nitzschioides*, spores of *Chaetoceros*, and *Actinoptychus vulgaris*, as well as of the open-ocean species *Thalassiosira lineata* and *Nitzschia interruptestriata.* Highest relative contribution of group 1 occurs at around 97–96 ka B.P. and between 92 and 62 ka B.P., and remains mostly below 25% after 62 ka B.P. (Figure 3b).

[21] Species with the highest score for group 2, which explains ~24% of the total variance, are the coastal *Cyclotella litoralis* accompanied by species thriving in oligotrophic-to-mesotrophic waters of low-latitude to midlatitude oceans such as *Azpeitia tabularis*, *Actinoptychus senarius*, *Rhizosolenia bergonii* and the tycoplanktonic *Paralia sulcata*. Group 2 mostly contributes during or close to HEs at around 82, 60–61, 46–47, 40, 26, and 14 and beyond 13 ka B.P. (Figure 3c).

[22] The pelagic, warm-water *Thalassionema nitzschioides* var. *parva* and resting spores of the coastal *Chaetoceros affinis* have the highest species scores for group 3, with secondary contributions of the pelagic *Thalassiosira ferelineata* and *Thalassionema frauenfeldii*, accompanied by the robust *Thalassiosira oestrupii* var. *oestrupii* and var. *venrickae*, and *Actinocyclus curvatulus*. Group 3 explains ~13% of the total variance and mainly contributes between 98 and 85, and 62 and 26 ka B.P. (Figure 3d).

[23] Group 4 is mainly composed of *Thalassionema pseudonitzschioides*, *Thalassiosira nanolineata*, and *Coscinodiscus radiatus*, and represents a mixed coastal and pelagic signal (8.6% of the total variance). Relative concentration of group 4 is highest between 64 and 56 ka B.P. Group 5 is a pelagic, warm-water assemblage dominated by *Fragilariopsis doliolus*, with minor contributions of open-ocean species *Alveus marinus, Thalassionema nitzschioides* var. *inflata*, *Azpeitia tabularis*, *Azpeitia barronii* and *Coscinodiscus decrecens* (4.1% of the total variance). Group 5 shows values below 20% for most of the record with a dramatic increase after 27 ka B.P.

## 5. Discussion

### 5.1. Millennial Timescale Variability of the Diatom Production in the Panama Basin

[24] MD02-2529 data for total diatom concentrations provide clear evidence for millennial variability in diatom production in the Panama Basin during the last glacial period (Figure 2). Minima of total diatom concentration broadly cooccurred with maxima in the oligotrophic assemblage from group 2 (Figures 3 and 4) and correspond to HEs (Figure 2; see also section 5.3) Such a pattern is also observed in the opal sedimentary content, a parameter not drastically affected by dissolution at MD02-2529 until ~18.5 ka B.P., as relatively good valve preservation suggests (Figures 2b and 2c). All together these results indicate that millennial-scale changes in diatom production closely followed the Heinrich-Dansgaard/Oeschger climate variability already recorded in the tropical Pacific hydrological characteristics and presumably linked to latitudinal migrations of the ITCZ [*Leduc et al.*, 2009]. Even though every millennial-scale event recognized in Greenland ice cores during the MIS3, 4 and 5 [*Bond et al.*, 1993] is not clearly mirrored by diatom values, maxima in total diatom concentration occurring during early MIS 4 as well as also during the MIS 4/3 transition and MIS 3 mimic Bond cycles and/or the SSS reconstruction derived from planktonic foraminifera at MD02-2529 (Figure 2), indicating a clear linkage between diatom production in the coastal EEP and rapid climate changes in the high-latitude North Atlantic.

[25] Diatom production in the Panama Basin is expected to respond to changes in surface water nutrient concentration as triggered by changes in wind conditions. The present-day

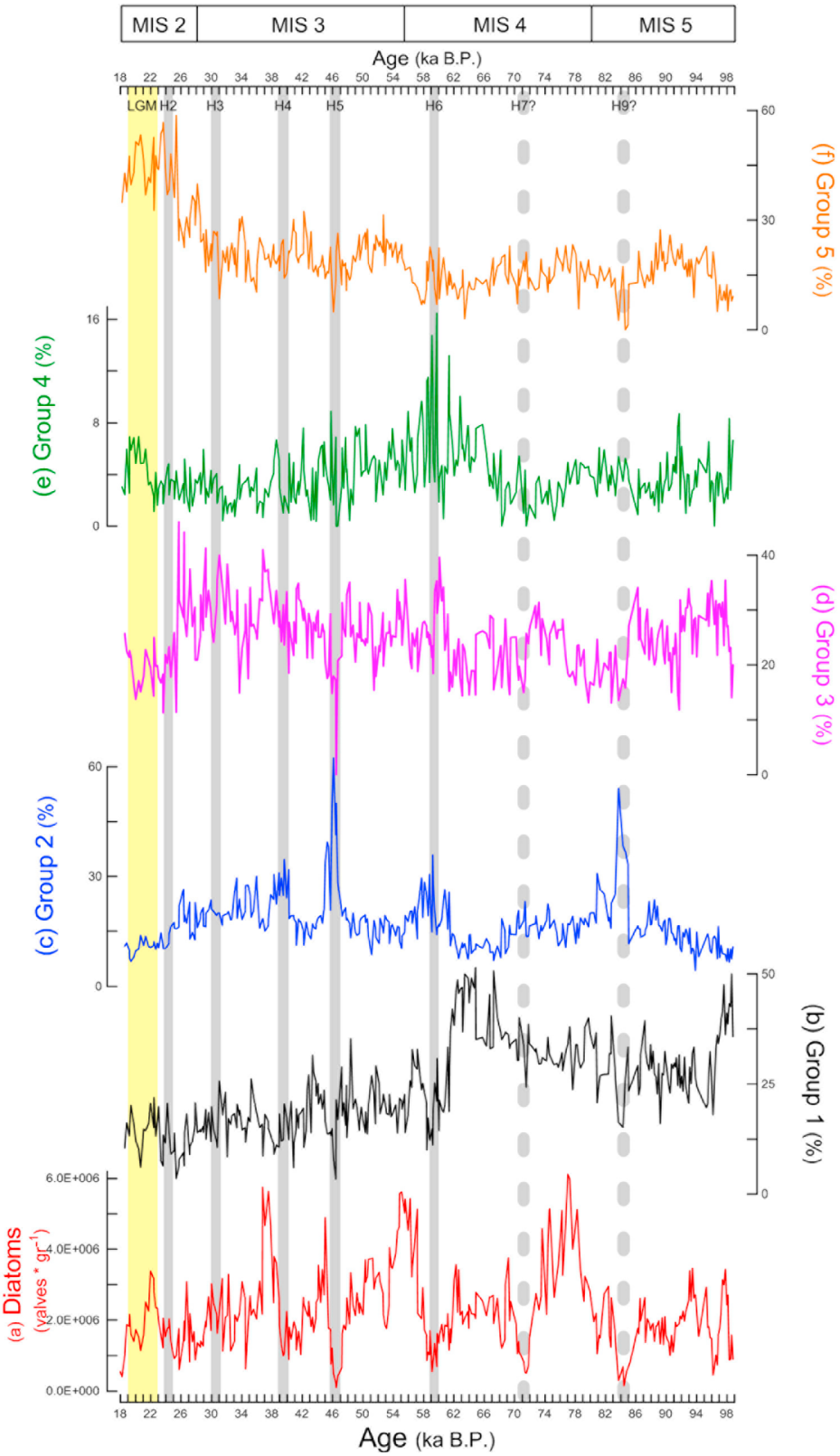


**Figure 3.** Downcore variations of (a) total diatom concentration (red line, valves $g^{-1}$) and the relative contribution of five diatoms groups (measured in percent): (b) Group 1 (black line), (c) Group 2 (blue line); (d) Group 3 (magenta line), (e) Group 4 (green line), and (f) Group 5 (orange line) at site MD02-2529 during the time period 98–18 ka B.P. For the qualitative composition of each group (factor) see Table 1. The Last Glacial Maximum (LGM, 23.0–19.0 ka B.P.) is indicated by the yellow shading and Heinrich events are indicated by the gray shadings.

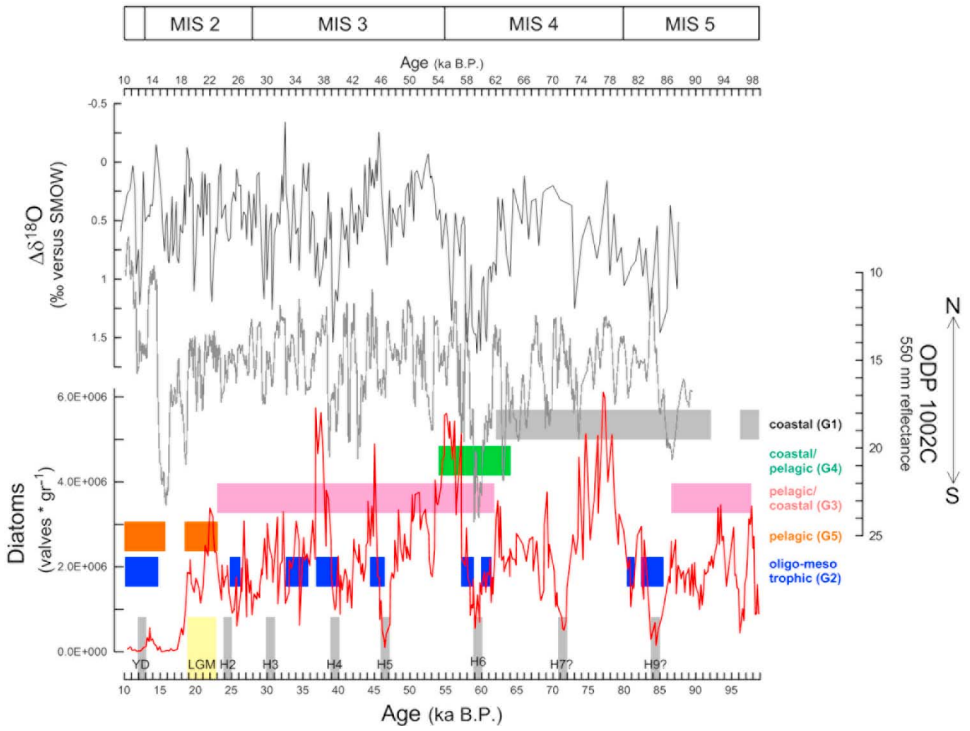


**Figure 4.** Summary of the peak occurrences of the diatom groups, as represented by horizontal color bars, at MD02-2529 during the time period 98–10 ka B.P. The horizontal shadings are Group 1 (gray), Group 2 (blue), Group 3 (pink), Group 4 (green), and Group 5 (orange). For the qualitative composition of each diatom group (factor) see Table 1. The measured color reflectance (550 nm) of Cariaco Basin sediments is from ODP Hole 1002C [*Peterson et al.*, 2000]. The value $\Delta\delta^{18}O$ (‰ versus SMOW) is a proxy for local seawater salinity at MD02-2529 [*Leduc et al.*, 2007]. The vertical shadings denote Heinrich events (H, gray) and the Last Glacial Maximum (LGM, yellow.)

diatom production along the southwestern Central American coast is heavily seasonal and strongly wind-dependant [*Fiedler*, 2002; *Pennington et al.*, 2006]. During July through October, as the ITCZ moves northward [*Amador et al.*, 2006], upwelling curl lifts the 10°N thermocline ridge across the entire Panama basin [*Kessler*, 2006] and the CRD develops west of MD02-2529 coring site (Figure 1). From November through January, the ITCZ migrates southward, and northeast trade winds blow strongly through Central American low-level mountain channels and trigger coastal upwelling northwest and southeast of MD02-2529 coring site [*Amador et al.*, 2006; *Fiedler*, 2002; *Kessler*, 2006] (see also section 2). These two distinct modes of atmospheric circulation are responsible for two distinct winter and summer spikes in organic matter fluxes to the seafloor in the Panama Basin [*Honjo*, 1982], and both are candidates for explaining the diatom productivity patterns on longer timescales.

[26] The relationship between higher diatom concentration and northernmost migration of the ITCZ during the last glacial period, as shown by the reflectance record at ODP Site 1002 in the Cariaco Basin (Figure 4), may explain the variability of the diatom production in the Panama Basin. Such atmospheric variability translated into the modern-day seasonal cycle corresponds to times when the CRD shoals and seeds most of the Panama Basin, hence inducing seasonal chlorophyll concentration maxima over site MD02-2529 (Figure 1). Such atmospheric conditions associated with northward migrations of the ITCZ might have been responsible for upwelling during periods when northern Panama Basin surface salinity was lowest (Figure 4).

[27] In addition to the ITCZ, persistent regional-scale winds blow through low-level mountain channels in the Central American narrow continental band [*Chelton et al.*, 2000; *Kessler*, 2006]. Opposite signs of wind stress curl generated by the Papagayo and Panama jets act to maintain local wind stress convergence at the MD02-2529 coring site, which is situated in the lee of the Talamanca Cordillera [*Chelton et al.*, 2000]. This local atmospheric pattern prevents coastal upwelling at the core location, as further suggested by a local SST maximum bracketed by coastal upwelling situated east and west of the MD02-2529 site [see *Pennington et al.*, 2006, Figure 6]. Such regional heterogeneity cannot change through time since it is linked to the topography of Central America. Therefore, increases in Papagayo and Panama coastal upwelling intensity as observed nowadays during winter may be valid for HEs since stronger northeastern trade winds are expected over these time periods [*Pahnke et al.*, 2007]. These local, rapid atmosphere-ocean interactions provide a potential explanation for why diatom production may have decreased at the MD02-2529 core location at these times, and may explain the absence of a glacial/interglacial pattern of variability in the diatom production as shown in downcore records from pelagic areas of the EEP [*Dubois et al.*, 2010].

### 5.2. Temporal Shifts of the Diatom Assemblage at Site MD02-2529

[28] The most prominent temporal trends in the diatom assemblage at MD02-2529, summarized now in Figure 4, are (1) the demise of diatom group 1 (predominantly coastal) after 62 ka B.P., (2) the highest contribution of diatom group 4 (coastal/pelagic) between 64 and 54 ka B.P., (3) the rise of diatom group 3 (pelagic/coastal) after 62 ka B.P., and (4) the rise of diatom group 5 (pelagic) after 27 ka B.P. The long-term succession of these four groups points to a longer trend from coastal diatoms, which predominantly occurred during MIS 5 and 4, toward pelagic diatoms, which occurred during MIS 3 and 2 in the Panama Basin (Figure 4). Apart from this first-order trend, there is a superimposed second-order variability displayed in the assemblages on a millennial timescale as well. This second-order pattern is expressed by increases in the relative contribution of diatom group 2 (coastal, oligo-mesotrophic) and cooccur with minima of opal content and diatom concentration that are concomitant with HEs (Figure 4; see also section 5.3).

[29] The prevalence of coastal diatoms between 98 and 62 ka B.P. (group 1, gray shading, Figure 4) is likely linked to the dominance of the CRCC over site MD02-2529 at these times. The neritic *Thalassionema nitzschioides* var. *nitzschioides*, which is the main component of group 1, represents boreal spring production in coastal areas of the low-latitude Pacific Ocean [*Sancetta*, 1992]; its dominance beyond surface waters of the upper continental slope indicates strong scattering of coastal waters into more pelagic areas [*Romero et al.*, 2008; *Romero and Armand*, 2010]. Toward the late MIS 4, the increase in the dominance of coastal/pelagic group 4 (green shading, Figure 4) at the expense of the neritic group 1 suggests a reorganization of regional surface ocean dynamics over the MD02-2529 site. Around 62 ka B.P., the increase in the relative contribution of the pelagic/coastal group 3 (pink shading, Figure 4) likely reveals the shoreward spreading of pelagic and hemipelagic waters with moderate nutrient content. This trend into more pelagic waters over site MD02-2529 continued well into the MIS 2 and the last deglaciation.

[30] The decrease in the total diatom concentration recorded after 18.5 ka B.P. corresponds to times when the dominance of nutrient-depleted water diatoms are the most expressed in the assemblages (groups 5 and 2, Figure 4). *Fragilariopsis doliolus*, the main contributor to group 5, mainly occurs in warm, nutrient-poor waters located along the southwestern coast of North America [*Romero and Armand*, 2010, and references therein] and is associated with gyre waters moving shoreward when the California Current relaxes during late summer and early fall [*Sancetta*, 1992; *Barron et al.*, 2003]. A similar decrease in diatom production after 20 ka B.P. has been already recorded in the Gulf of California [*Sancetta*, 1992]. Such features can probably be linked to similar features identified upstream along the California margin during periods of glacial maxima [*Herbert et al.*, 2001]. The strong reduction in diatom values, the marked shift in species composition and the poor valve preservation after the LGM (Figures 2 and 4) together point toward the dominance of warmer waters and an increasingly stratified upper water column over the MD02-2529 site. Although opal fluxes at MD02-2529 are not Al- or Th-normalized, we assume here that the abrupt decrease in sedimentary opal content after the LGM differs from those recorded in pelagic EEP locations. Within the EEP, opal/Al values [*Kienast et al.*, 2006; *Dubois et al.*, 2010] and Th-normalized opal fluxes [*Bradtmiller et al.*, 2006] suggest that diatom productivity was lower during LGM as compared to the deglaciation. Pelagic EEP sites, however, are not necessarily impacted by the same processes as at MD02-2529 site which is much closer to the Central American margin (see also discussion by *Dubois et al.* [2010]).

[31] The abrupt decrease in the valve preservation recorded after the LGM in the coastal Panama Basin (Figure 2) agrees well with observations in the pelagic EEP at Site 849 (i.e., at ~110°W near the equator). Based on the electron microscopy surveys of valves of the well-silicified *Azpeitia nodulifera*, *Warnock et al.* [2007] observed stronger valve dissolution during the deglaciation than earlier during LGM. Our observations, however, contrast with those recently presented by *Dubois et al.* [2010]. Using geochemical proxies in a series of sediment cores from pelagic areas of the tropical eastern Pacific, *Dubois et al.* [2010] offered evidence of enhanced opal preservation during deglaciation. This contradiction can be partly explained by the use of different proxies: while *Warnock et al.* [2007] and the present study characterized the valve preservation with microscopy observations, while *Dubois et al.* [2010] used biogeochemical proxies. Since only one study assessing the preservation of diatom remains in the pelagic EEP is available so far [*Warnock et al.*, 2007], further studies of species composition and valves preservation at other EEP core locations are required to assess whether the deglaciation was more or less corrosive with respect to opal.

### 5.3. Global Hydrographic Changes and the Diatom Paleoproduction in the Panama Basin

[32] One of the most remarkable features observed in diatom production recorded in MD02-2529 sediments is the dramatic decrease observed during HEs. To explain the low diatom production recorded during HEs in the Northern Hemisphere oceans, two opposite hypotheses have been proposed. The first hypothesis interprets the low diatom concentration during HEs as a consequence of the drastic decrease in surface water productivity [*Nave et al.*, 2007]. The second hypothesis, however, considers that diatom productivity increased, probably in response to enhanced nutrient input from the continents, and that this increase would not have been recorded in the sediments [*Sancetta*, 1992]. Drastic increases in nutrient-depleted water diatom assemblages coeval with decreases in diatom counts recorded at site MD02-2529 favor the hypothesis that the low diatom concentrations during HEs 6 to 3 mirrors abrupt decreases in the diatom production in the Panama Basin (Figure 3). It would additionally suggest a reduced CRD activity over these time intervals despite increased Tehuantepec, Papagayo and Panama northeast wind jets. Such a hypothesis is in line with a regional ocean-atmosphere model from Central America that accurately simulates the seasonal cycle of atmospheric and oceanic circulation in the region [*Xie et al.*, 2007] and further points to increased wind jets and decreased CRD activity in water hosing experiments [*Pahnke et al.*, 2007].

[33] Water hosing experiments using earth system models of intermediate complexity that incorporate changes in the carbon cycle, in nutrient availability and in the response of phytoplankton communities provide further diagnostics for changes in the EEP productivity during HEs [*Schmittner et al.*, 2007; *Menviel et al.*, 2008]. These models indicate that the reduction in the Atlantic Meridional Overturning Circulation (AMOC) caused a year-round halocline in surface waters overlying site MD02-2529, a reduction in the nutrients supplied by upwelled waters and strong variations in export production over broad geographic regions without significant time lags [*Schmittner et al.*, 2007; *Menviel et al.*, 2008]. Other simulations suggest that the upwelled water in equatorial regions of the oceans originated from the subtropics during HEs, as circulation in the Pacific Ocean was dominated by subtropical cells [*Haarsma et al.*, 2008]. The global reduction in the amount of water upwelled together with changes in the source of upwelling water led to a reduction in the nutrient content in the upper 1000 m and to a nutrient accumulation in the deep ocean during HEs [*Menviel et al.*, 2008].

[34] Such hydrological effects simulated for HEs agree well with abrupt changes in the dominance of diatom populations at MD02-2529. In addition to the decrease of diatom and opal concentrations during HEs, maxima of the well-silicified diatom *C. litoralis* (group 2, blue shading, Figure 4) reflect stratified, nutrient-limited waters. A present-day analog is given by a 3 year sediment trap study carried out in the Gulf of California where *C. litoralis* was dominant during summers, that is, when the lithogenic flux is high and opal values are low [*Sancetta*, 1995]. Evidence previously attained at MD02-2529 relates the southernmost migration of the ITCZ with SSS increases during HEs [*Leduc et al.*, 2007, 2009]. Associated water column stratification over site MD02-2529 possibly limited the input of nutrients into the euphotic zone, leading to a diatom production decrease. Additionally, the poorest valve preservation during HEs (Figure 2) also suggests $H_4SiO_4$-depleted surface waters in the Panama Basin at these times.

[35] The predominant explanation for opal variations along the pelagic EEP has been the silica leakage hypothesis [e.g., *Brzezinski et al.*, 2002; *Matsumoto et al.*, 2002]. It has been speculated that during glacial periods the excess $H_4SiO_4$ was transported from the Southern Ocean to lower latitudes within Subantarctic Mode Waters [*Matsumoto et al.*, 2002]. Subsequently, *Chase et al.* [2003] suggested that high-latitude sea ice cover was the prime factor responsible for reduced Si utilization in glacial Antarctic surface waters. Compared to the pelagic locations along the EEP, piston core MD02-2529 was collected in an area affected by a variety of processes such as seasonal changes in upwelling and wind intensity, and depth variations of the thermocline (see section 2). The comparison of opal records from the pelagic EEP with that of MD02-2529 delivers some insights into the nutrient dynamics of the low-latitude Pacific as a whole. The weak temporal relationship between opal records from MD02-2529 and more pelagic zones [*Kienast et al.*, 2006; *Bradtmiller et al.*, 2006, 2010; *Dubois et al.*, 2010] still needs to be tested and requires a denser net of cores situated between the Panama Basin and the pelagic EEP. In addition, it also requires the assessment of the quantitative variations in the diatom assemblages in pelagic EEP locations.

[36] The low correlation between total diatom concentration and valve preservation ($R = 0.38$) suggests that the preserved diatom signal at site MD02-2529 weakly depends on the species composition of the diatom assemblage. *Pichevin et al.* [2009] proposed that the Si- and Fe-replete conditions in the EEP during the LGM led to lowered Si utilization and diatom silicification, which may further have favored dissolution of opal. Although this hypothesis might be valid for the pelagic EEP, there is no clear evidence for long-term opal burial changes on the glacial-interglacial timescale at site MD02-2529 prior to the LGM. Our results indicate that coastal areas surrounding the Panama Basin were less affected by large-scale process such as nutrient export from high latitudes into pelagic areas from the EEP during the last glacial cycle. We therefore suggest that local hydrological variability induced by atmospheric circulation changes, potentially exacerbated by other large-scale processes such as those identified in water hosing experiments, best explains our diatom records that differ from those recorded in more pelagic areas.

## 6. Concluding Remarks

[37] Our high-resolution record of the diatom production provides evidence for millennial timescale variability in total diatom production and the species composition of the diatom community in the coastal Panama Basin during the last glacial cycle. Reduced diatom production during HEs are best explained by the response to the slowdown of the AMOC and local variability in the nutrient input due to changes in upwelling intensity, wind speed and/or wind direction along the Central American coastline.

[38] Since features observed at site MD02-2529 do not share the glacial-interglacial pattern of variability observed in pelagic EEP sites, the reconstruction of diatom production in the Panama Basin indicates that nutrient and hydrological variability in coastal areas from the low-latitude eastern Pacific may not respond as in more pelagic areas. Diatom data from site MD02-2529 highlight, however, how local productivity interacts with hydrological changes triggered by atmospheric variability, which may have been pivotal for driving local changes in the thermocline structure.

[39] The mixed pelagic/coastal diatom assemblage shows that site MD02-2529 lays in a transition zone between neritic and open-ocean surface waters. Two major long-term shifts in the composition of the diatom assemblages, between 64 and 54 ka B.P. and after the LGM, suggest that a large, persistent and pervasive drift in assemblages from coastal to pelagic environmental settings occurred in the Panama Basin. Such long-term trends, however, cannot explain the most prominent features of diatom valve concentrations that occurred at the millennial timescale. The pattern of increases and decreases in total diatom concentration is independently supported by shifts in the diatom assemblages that reveal changes in the hydrologic conditions over the Panama Basin at the millennial timescale.

[40] The warming of surface waters after the LGM induced an increase in stratification that, in turn, reduced the vertical transport and mixing of cooler subsurface, more nutrient-rich waters. The shoreward spreading of waters

with low nutrient ($H_4SiO_4$) content shortly after the LGM led to oligotrophic surface conditions in the Panama Basin, and consequently lowered the diatom production and enhanced dissolution of valves.

[41] **Acknowledgments.** This research was supported by grants to OER by the Spanish Council of Scientific Research (MICIN-20073MA110). We acknowledge support from INSU and the French Polar Institute IPEV, which provided the R/V *Marion Dufresne* and the CALYPSO coring system used during the IMAGES VIII MONA cruise. Paleoclimate work at CEREGE is supported by grants from the CNRS, the ANR, and the Gary Comer Science and Education Foundation. We thank Marco Klann and Eva Kwoll (MARUM, Bremen, Germany) and Barbara Diaz (IACT, Granada, Spain) for their lab work. Reviews by Rebecca Robinson and an anonymous reviewer greatly improved this work. Comments by Editor Christopher Charles are also acknowledged. Leah Schneider (Penn State University) improved the English language.

## References

Amador, J. A., E. J. Alfaro, O. G. Lizano, and V. O. Magaña (2006), Atmospheric forcing of the eastern tropical Pacific: A review, *Prog. Oceanogr.*, *69*, 101–142, doi:10.1016/j.pocean.2006.03.007.

Barron, J. A., and D. Bukry (2007), Development of the California Current during the past 12,000 yr based on diatoms and silicoflagellates, *Palaeogeogr. Palaeoclimatol. Palaeoecol.*, *248*, 313–338, doi:10.1016/j.palaeo.2006.12.009.

Barron, J. A., L. Heusser, T. Herbert, and M. Lyle (2003), High-resolution climatic evolution of coastal northern California during the past 16,000 years, *Paleoceanography*, *18*(1), 1020, doi:10.1029/2002PA000768.

Barron, J. A., D. Bukry, and W. E. Dean (2005), Paleoceanographic history of the Guaymas Basin, Gulf of California, during the past 15,000 years based on diatoms, silicoflagellates, and biogenic sediments, *Mar. Micropaleontol.*, *56*, 81–102, doi:10.1016/j.marmicro.2005.04.001.

Bond, G. C., W. Broecker, S. Johnsen, J. McManus, L. Labeyrie, J. Jouzel, and G. Bonani (1993), Correlations between climate records from North Atlantic sediments and Greenland ice, *Nature*, *365*, 143–147, doi:10.1038/365143a0.

Bradtmiller, L. I., R. F. Anderson, M. Q. Fleisher, and L. H. Burckle (2006), Diatom productivity in the equatorial Pacific Ocean from the last glacial period to the present: A test of the silicic acid leakage hypothesis, *Paleoceanography*, *21*, PA4201, doi:10.1029/2006PA001282.

Bradtmiller, L. I., R. F. Anderson, M. Q. Fleisher, and L. H. Burckle (2009), Comparing glacial and Holocene opal fluxes in the Pacific sector of the Southern Ocean, *Paleoceanography*, *24*, PA2214, doi:10.1029/2008PA001693.

Bradtmiller, L. I., R. F. Anderson, J. P. Sachs, and M. Q. Fleisher (2010), A deeper respired carbon pool in the glacial equatorial Pacific ocean, *Earth Planet. Sci. Lett.*, *299*, 417–425, doi:10.1016/j.epsl.2010.09.022.

Brzezinski, M. A., et al. (2002), A switch from $Si(OH)_4$ to $NO_3^-$ depletion in the glacial Southern Ocean, *Geophys. Res. Lett.*, *29*(12), 1564, doi:10.1029/2001GL014349.

Chase, Z., R. F. Anderson, M. Q. Fleisher, and P. W. Kubik (2003), Accumulation of biogenic and lithogenic material in the Pacific sector of the Southern Ocean during the past 40,000 years, *Deep Sea Res., Part II*, *50*, 799–832, doi:10.1016/S0967-0645(02)00595-7.

Chelton, D. B., M. H. Freilich, and S. K. Esbensen (2000), Satellite observations of the wind jets off the Pacific coast of Central America. Part II: Regional relationships and dynamical considerations, *Mon. Weather Rev.*, *128*, 2019–2043, doi:10.1175/1520-0493(2000)128<2019:SOOTWJ>2.0.CO;2.

Cortese, G., R. Gersonde, C.-D. Hillenbrand, and G. Kuhn (2004), Opal sedimentation shifts in the World Ocean over last 15 Myr, *Earth Planet. Sci. Lett.*, *224*, 509–527, doi:10.1016/j.epsl.2004.05.035.

DeMaster, D. J. (1981), The supply and accumulation of silica in the marine environment, *Geochim. Cosmochim. Acta*, *45*, 1715–1732, doi:10.1016/0016-7037(81)90006-5.

Dubois, N., M. Kienast, S. Kienast, S. E. Calvert, R. François, and R. F. Anderson (2010), Sedimentary opal records in the Eastern Equatorial Pacific: It's not all about leakage, *Global Biogeochem. Cycles*, *24*, GB4020, doi:10.1029/2010GB003821.

Fiedler, P. C. (2002), The annual cycle and biological effects of the Costa Rica Dome, *Deep Sea Res., Part I*, *49*, 321–338, doi:10.1016/S0967-0637(01)00057-7.

Fiedler, P. C., and L. D. Talley (2006), Hydrography of the eastern tropical Pacific: A review, *Prog. Oceanogr.*, *69*, 143–180, doi:10.1016/j.pocean.2006.03.008.

Haarsma, R. J., E. Campos, W. Hazeleger, and C. Severijns (2008), Influence or the meridional overturning circulation on the tropical Atlantic climate and variability, *J. Clim.*, *21*, 1403–1416, doi:10.1175/2007JCLI1930.1.

Herbert, T. D., et al. (2001), Collapse of the California current during glacial maxima linked to climate change on land, *Science*, *293*, 71–76, doi:10.1126/science.1059209.

Honjo, S. (1982), Seasonality and interaction of biogenic and lithogenic particulate flux at the Panama Basin, *Science*, *218*, 883–884, doi:10.1126/science.218.4575.883.

Kessler, W. S. (2006), The circulation of the eastern tropical Pacific: A review, *Prog. Oceanogr.*, *69*, 181–217, doi:10.1016/j.pocean.2006.03.009.

Kienast, S. S., M. Kienast, S. Jaccard, S. E. Calvert, and R. François (2006), Testing the silica leakage hypothesis with sedimentary opal records from the eastern equatorial Pacific over the last 150 kyrs, *Geophys. Res. Lett.*, *33*, L15607, doi:10.1029/2006GL026651.

Lea, D., D. K. Pak, L. C. Peterson, and H. A. Hughen (2003), Synchroneity of tropical and high-latitude Atlantic temperatures over the Last Glacial Termination, *Science*, *301*, 1361–1364, doi:10.1126/science.1088470.

Leduc, G., L. Vidal, K. Tachikawa, F. Rostek, C. Sonzogni, L. Beaufort, and E. Bard (2007), Moisture transport across Central America as a positive feedback on abrupt climatic changes, *Nature*, *445*, 908–911, doi:10.1038/nature05578.

Leduc, G., L. Vidal, K. Tachikawa, and E. Bard (2009), ITCZ rather than ENSO signature for abrupt climate changes across the tropical Pacific?, *Quat. Res.*, *72*, 123–131, doi:10.1016/j.yqres.2009.03.006.

Leduc, G., L. Vidal, K. Tachikawa, and E. Bard (2010), Changes in Eastern Pacific ocean ventilation at intermediate depth over the last 150 kyr BP, *Earth Planet. Sci. Lett.*, *298*, 217–228, doi:10.1016/j.epsl.2010.08.002.

Leynaert, A., P. Tréguer, C. Lancelot, and M. Rodier (2001), Silicon limation of biogenic silica production in the Equatorial Pacific, *Deep Sea Res., Part I*, *48*, 639–660, doi:10.1016/S0967-0637(00)00044-3.

Lisiecki, L. E., and M. E. Raymo (2005), A Pliocene-Pleistocene stack of 57 globally distributed benthic $\delta^{18}O$ records, *Paleoceanography*, *20*, PA1003, doi:10.1029/2004PA001071.

Matsumoto, K., J. L. Sarmiento, and M. A. Brzezinski (2002), Silicic acid leakage from the Southern Ocean: A possible explanation for glacial atmospheric $pCO_2$, *Global Biogeochem. Cycles*, *16*(3), 1031, doi:10.1029/2001GB001442.

Menviel, L., A. Timmermann, A. Mouchet, and O. Timm (2008), Meridional reorganizations of marine and terrestrial productivity during Heinrich events, *Paleoceanography*, *23*, PA1203, doi:10.1029/2007PA001445.

Müller, P., and R. R. Schneider (1993), An automated leaching method for the determination of opal in sediments and particulate matter, *Deep Sea Res., Part I*, *40*, 425–444, doi:10.1016/0967-0637(93)90140-X.

Nave, S., L. Labeyrie, J. Gherardi, N. Caillon, E. Cortijo, C. Kissel, and F. Abrantes (2007), Primary productivity response to Heinrich events in the North Atlantic Ocean and Norwegian Sea, *Paleoceanography*, *22*, PA3216, doi:10.1029/2006PA001335.

Pahnke, K., J. P. Sachs, L. Keigwin, A. Timmermann, and S.-P. Xie (2007), Eastern tropical Pacific hydrologic changes during the past 27,000 years from D/H ratios in alkenones, *Paleoceanography*, *22*, PA4214, doi:10.1029/2007PA001468.

Pennington, T. P., K. L. Mahoney, V. S. Kuwahara, D. D. Kolber, R. Calienes, and F. P. Chavez (2006), Primary production in the eastern tropical Pacific: A review, *Prog. Oceanogr.*, *69*, 285–317, doi:10.1016/j.pocean.2006.03.012.

Peterson, L. C., G. H. Haug, K. A. Hughen, and U. Röhl (2000), Rapid changes in the hydrologic cycle of the tropical Atlantic during the Last Glacial, *Science*, *290*, 1947–1951, doi:10.1126/science.290.5498.1947.

Pichevin, L. E., B. C. Reynolds, R. S. Ganeshram, I. Cacho, L. Pena, K. Keefe, and R. M. Ellam (2009), Enhanced carbon pump inferred from relaxation of nutrient limitation in the glacial ocean, *Nature*, *459*, 1114–1117, doi:10.1038/nature08101.

Póveda, G., P. R. Waylen, and R. S. Pulwarty (2006), Annual and interannual variability of the present climate in the northern South America and southern Mesoamerica, *Palaeogeogr. Palaeoclimatol. Palaeoecol.*, *234*, 3–27, doi:10.1016/j.palaeo.2005.10.031.

Ragueneau, O., et al. (2000), A review of the Si cycle in the modern ocean: Recent progress and missing gaps in the application of biogenic opal as a paleoproductivity proxy, *Global Planet. Change*, *26*, 317–365, doi:10.1016/S0921-8181(00)00052-7.

Robinson, R. S., D. S. Sigman, P. J. DiFiore, M. M. Rhode, T. A. Mashiotta, and D. L. Lea (2005), Diatom-bound $^{15}N/^{14}N$: New support for enhanced nutrient consumption in the ice age subantarctic, *Paleoceanography*, *20*, PA3003, doi:10.1029/2004PA001114.

Romero, O. E., and L. K. Armand (2010), Marine diatoms as indicators of modern changes in oceanographic conditions, in *The Diatoms, Applications for the Environmental and Earth Sciences*, 2nd ed., edited by

J. P. Smol and E. F. Stoermer, pp. 373–400, Cambridge Univ. Press, Cambridge, U. K.

Romero, O. E., J.-H. Kim, and B. Donner (2008), Submillennial-to-millennial variability of diatom production off Mauritania, NW Africa, during the last glacial cycle, *Paleoceanography*, *23*, PA3218, doi:10.1029/2008PA001601.

Sancetta, C. (1992), Comparison of phytoplankton in sediment trap time series and surface sediments along a productivity gradient, *Paleoceanography*, *7*, 183–194, doi:10.1029/92PA00156.

Sancetta, C. (1995), Diatoms in the Gulf of California: Seasonal flux patterns and the sediment record for the last 15,000 years, *Paleoceanography*, *10*, 67–84, doi:10.1029/94PA02796.

Schmittner, A., E. D. Galbraith, S. W. Hostetler, T. F. Pedersen, and R. Zhang (2007), Large fluctuations of dissolved oxygen in the Indian and Pacific oceans during Dansgaard-Oeschger oscillations caused by variations of North Atlantic Deep Water subduction, *Paleoceanography*, *22*, PA3207, doi:10.1029/2006PA001384.

Schrader, H.-J., and R. Gersonde (1978), Diatoms and silicoflagellates, in *Micropaleontological Counting Methods and Techniques: An Exercise on an Eight Metres Section of the Lower Pliocene of Capo Rosello, Sicily*, edited by W. J. Zachariasse et al., *Utrecht Micropaleontol. Bull.*, 17, 129–176.

Takahashi, T., et al. (1997), Global air-sea flux of $CO_2$: An estimate based on measurements of sea–air $pCO_2$ difference, *Proc. Natl. Acad. Sci. U. S. A.*, *94*(16), 8292–8299, doi:10.1073/pnas.94.16.8292.

Warnock, J., R. Scherer, and P. Loubere (2007), A quantitative assessment of diatom dissolution and late quaternary primary productivity in the Eastern Equatorial Pacific, *Deep Sea Res., Part II*, *54*, 772–783, doi:10.1016/j.dsr2.2007.01.011.

Willett, C. S., R. R. Leben, and M. F. Lavín (2006), Eddies and Tropical instability waves in the eastern tropical Pacific: A review, *Prog. Oceanogr.*, *69*, 218–238, doi:10.1016/j.pocean.2006.03.010.

Wyrtki, K. (1966), Oceanography of the eastern equatorial Pacific Ocean, *Oceanogr. Mar. Biol. Annu. Rev.*, *4*, 33–68.

Xie, S.-P., et al. (2007), A regional ocean-atmosphere model for eastern Pacific climate: Toward reducing tropical biases, *J. Clim.*, *20*, 1504–1522, doi:10.1175/JCLI4080.1.

G. Fischer, Faculty of Geosciences and MARUM, University of Bremen, Klagenfurter/Leobener Strasse, D-28359 Bremen, Germany.

G. Leduc, Universität Kiel, Ludewig-Meyn-Straße 10, D-24118 Kiel, Germany.

O. E. Romero, Instituto Andaluz de Ciencias de la Tierra (CSIC-UGR), Campus Fuentenueva, Facultad de Ciencias, Universidad de Granada, E-18002 Granada, Spain. (oromero@ugr.es)

L. Vidal, CEREGE, UMR6635, CNRS Université Paul Cézanne Aix-Marseille III, Europôle de l'Arbois, BP 80, F-13545 Aix-en-Provence CEDEX 04, France.